applied sciences

MDPI

Article

Experimental and Mathematical Study of Flexible–Rigid Rail Vehicle Riding Comfort and Safety

Sunil Kumar Sharma [1], Rakesh Chandmal Sharma [2], Yeongil Choi [3] and Jaesun Lee [4,*]

[1] School of Engineering & Applied Science, Gati Shakti Vishwavidyalaya, Vadodara 390004, India
[2] Mechanical Engineering Department, Graphic Era (Deemed to be University), Dehradun 248002, India
[3] Department of Smart Manufacturing Engineering, Changwon National University, Changwon 51140, Republic of Korea
[4] School of Mechanical Engineering, Changwon National University, Changwon 51140, Republic of Korea
* Correspondence: jaesun@changwon.ac.kr

Abstract: This paper analyses the dynamic behavior of a rail vehicle using experimental and simulation analysis on a multi-rigid–flex body model. The mathematical models are developed considering the car body, bogie frame, and wheel axle for rail vehicles of rigid–flexible and multi-rigid formulations, taking the car body as rigid for the rigid body analysis and the flexible car body for flex–rigid analysis. A finite element model of the car body was developed in ANSYS, and substructure and modal analyses were performed. The mathematical model is validated through an experiment conducted by the Research Design and Standards Organization. Then, the validated model is further analyzed to evaluate the running comfort, using the Sperling ride index and the running safety, by investigating the derailment coefficient and wheel load reduction rate. The impact of flexibility on the vehicle's running stability is investigated using the rigid body dynamics model and experimental data. Compared to experimental data, the simulation results reveal that elastic vibration cannot be neglected in vehicle dynamics, since the rigid–flexible coupling model is slightly more significant than the rigid-body model for ride comfort and safety.

Keywords: rigid; car body; flexible; comfort; safety

check for updates

Citation: Sharma, S.K.; Sharma, R.C.; Choi, Y.; Lee, J. Experimental and Mathematical Study of Flexible–Rigid Rail Vehicle Riding Comfort and Safety. *Appl. Sci.* **2023**, *13*, 5252. https://doi.org/10.3390/app13095252

Academic Editor: Diogo Ribeiro

Received: 27 February 2023
Revised: 17 April 2023
Accepted: 20 April 2023
Published: 22 April 2023

1. Introduction

A rigid–flexible analysis is a numerical simulation used to model the dynamic behaviors of complex systems with rigid and flexible components. In the case of rail vehicles, this type of analysis can be used to simulate the vehicle's behavior as it travels along the track. The rigid components of the rail vehicle include the wheels, axles, and main frame. These components are modelled as rigid bodies that move together as a single unit. The flexible members have a suspension system, body, and other elements designed to deform or flex under load [1].

The system is modelled using a combination of mathematical equations and computer simulations to perform a rigid–flexible analysis of a rail vehicle. The simulation considers the forces acting on the vehicle as it travels along the track, including the vehicle's weight, the forces generated by the propulsion system, and the forces generated by the suspension system. The simulation also takes into account the deformation of the flexible components of the vehicle, which can have a significant impact on the vehicle's behaviors. By analyzing the vehicle's behaviors under different conditions, engineers can optimize the vehicle's design to improve performance, safety, and efficiency. A rigid–flexible analysis is a powerful tool for designing and optimizing rail vehicles. By simulating the vehicle's behaviors under various conditions, engineers can identify potential issues and make design changes before the vehicle is built, saving time and money in the long run.

In railway vehicles, the vibrations mainly generated due to wheel-rail interaction are isolated by the vehicle suspension system before being transferred to the car body. The car body's vertical vibrations arise mainly due to the vertical–lateral irregularities of the track, and also due to the wheel's profile. After hundreds of hours of running on tracks, some wheels lose their correct profile; they start to present wear and generate vibrations. These are incorporated by simple eigenmodes of rigid vehicle masses, i.e., vertical and pitch modes [2]. A continuous effort has been applied by rail dynamics researchers to improve rail vehicle performance indices, i.e., stability, ride, and curving ability [3]. Considering different models, researchers have optimized ride comfort and other performance indices of rail and road vehicles, i.e., vehicle power performance, energy consumption, regenerated power, road holding, etc. [4]. It has been found in the past that the design of railway passenger vehicles has conflicting requirements to obtain maximum ride comfort and minimum track deterioration, as the wheels are affected first, and their profile needs to be corrected on big lathes and maximum payload. Compound structural modes are included due to car body flexibility, i.e., bending and twisting modes. Past research has suggested that a 5 to 10 Hz resonating frequency significantly affects car body vibrations in a symmetrical bending mode [5]. This frequency range is critical to human comfort sensitivity. In this car body, structural vibrations in the bending mode arise in a lightweight structure and are responsible for poor vehicle ride comfort [6].

Control of car body vibrations may be accomplished in several different ways. An essential contrast may be drawn between the approaches concentrating on the flexible car body modes' control and those considering the rigid body modes. This distinction applies to all of these systems. It is possible to lessen the effects of the first flexible car body modes using piezoelectric actuators and technology that provides suspended mass control. Piezo-stack actuators were used to demonstrate the solution's efficacy via experimental testing on a 1:10 scale model and co-simulations for a complete vehicle [7]. Using a 1:6 scaled Shinkansen vehicle, Kamada et al. [8] demonstrated that the efficacy of a combination of piezo-stack and linear actuators may be improved upon. As shown by Huang et al. [9], the suspended equipment divides the first bending frequency into two frequencies with lesser amplitudes. This equipment includes traction transformers, power converter units, fan systems, etc. The active control of the suspended mass is an improvement that may be made using this method. Foo et al. [10] researched the impact of regulating a suspended group placed on a beam-like car body model using an electromagnetic actuator. Wang et al. [11] stated this method's benefits when used for semi-active suspensions.

Despite their efficacy in regulating flexible body modes, the approaches described above have marginal influence on controlling stiff body modes, which still affect ride comfort. The method of control used most often falls into the second group. With this configuration, traditional dampers are replaced by actuators [12] situated between the bogies (also known as wheelsets) and the car body in vertical and lateral directions. Inter-vehicle actuators (and lateral–vertically linked actuators) are not included in these designs [13].

A lower-weight design of railway vehicles aims to achieve higher speeds with lesser power requirements. It also results in a decrease in ground vibration and a reduction in construction costs. It is also recommended that the car body's lightweight design fulfils other objectives such as crashworthiness, strength and wear. Researchers have conducted extensive analyses on car body structural vibrations that seriously affect the vehicle ride comfort, and the influences of active and semi-active secondary suspensions on vehicle vibration isolation, considering the flexibility of the car body [14]. Researchers have also determined the influences of active secondary suspensions and an active DVA attached to the car body to attenuate flexible and rigid mode vibration [15–17]. Increasing the vehicle speed significantly increases the energy and frequency range of the track inputs, which induces the flexural vibrations in the car body. It has also been found that typical track excitation frequencies and vehicle speeds extensively boost the car body vibration modes [13].

In recent years, much theoretical research has been conducted to identify effective strategies for reducing the flexible vibrations that cause discomfort in railway vehicle passengers. Numerical simulation programs have been utilized to analyze and assess the comfort performance of railway vehicles based on specific theoretical models of the vehicles. The accuracy of these models largely depends on the quality of the car body modelling. One such theoretical model is the "stiff car body", which provides insights into the fundamental features of vibration behaviors in railway vehicles. The findings from these models suggest that the ends of the car body are the most critical areas in ride comfort. However, in reality, there are instances in which the level of vibrations measured at the center of the car body is equivalent to the level recorded at either end, despite the importance of the ends [7]. It is important to note that passenger comfort is a significant factor in this research. Passengers experience heightened discomfort at specific vibration frequencies and for particular durations. Therefore, reducing these flexible vibrations is crucial for enhancing passenger comfort and satisfaction during train journeys.

This paper investigates a dynamics analysis of rail vehicle behaviors using experimental and numerical techniques. The focus is on investigating the impact of elastic vibrations on rail vehicle dynamics. Mathematical models are developed for the car body, bogie frame, and wheel axle using rigid–flexible and multi-rigid formulations. For the rigid body analysis, the car body is considered rigid, while a flexible car body is considered for the flex–rigid analysis. ANSYS is used to build a finite element model for the car body, and substructure and modal analyses are carried out. The dynamic simulation and numerical analysis are then validated using experimental results. The study also evaluates the running comfort and safety of the rail vehicle. The Sperling Ride Index measures running comfort at the rigid and flexible car body center. In contrast, the calculation error of running safety is assessed using the mean derailment coefficient and mean wheel load-reduction rate.

2. Rail Vehicle Mathematical Modelling

For modelling and simulation, a full-size Indian railway ICF coach is studied [6]. For mathematical modelling, the two bogies, car body and four wheelsets are considered connected by the suspension system, as shown in Figure 1. The car body may be described using a Euler–Bernoulli type free–free equivalent beam. This beam has a constant section, and its mass is spread uniformly.

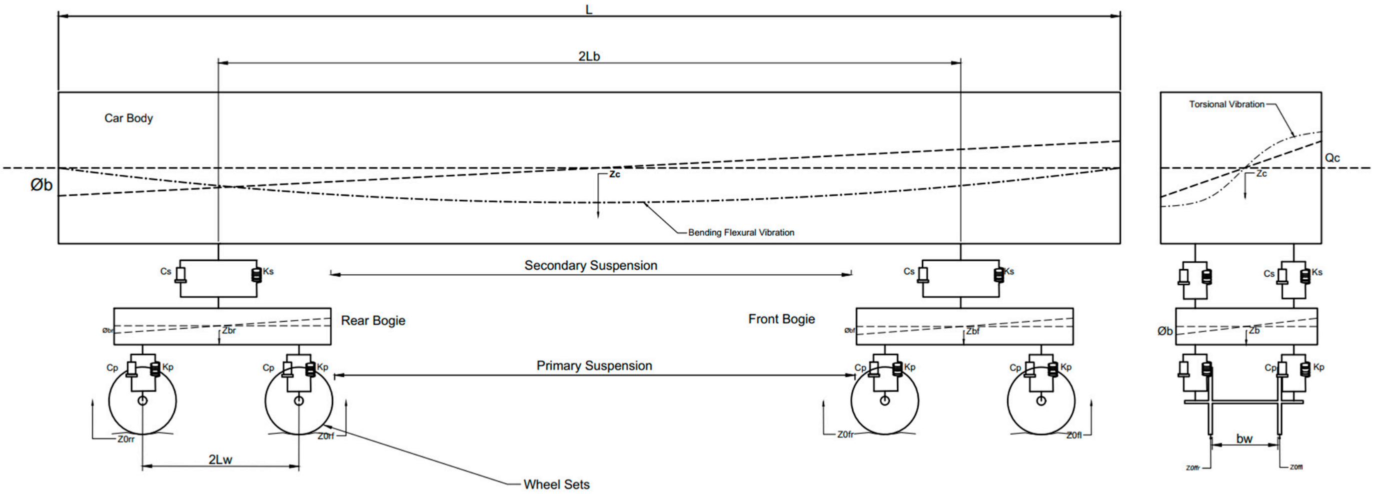

Figure 1. ICF coach mathematical model.

2.1. Flexural Motion Equations

Euler–Bernoulli beam theory of the free–free type is utilized for the bending and torsional vibration of the car body. Equation (1) is used to evaluate the vibration due to bending [18].

$$EI\frac{\partial^4 v(x,t)}{\partial x^4} + \rho_b A_b \frac{\partial^2 v(x,t)}{\partial t^2} + C_i \frac{\partial v(x,t)}{\partial t} = -f_{sfr}\delta\left(x - x_f\right) - f_{sfl}\delta\left(x - x_f\right) - f_{srr}\delta(x - x_r) - f_{srl}\delta(x - x_r) \quad (1)$$

where $f_{sfr}, f_{sfl}, f_{srr}$ and f_{srl} are the forces induced by the secondary suspensions (represented by the first subindex s) on the car body. The second and the third subindices represent the front (f) or the rear (r) wheelset and the left (l) or the right (r) wheel, respectively.

Modes due to bending for unsupported beams can be calculated as

$$X_n(x) = \cos\ \beta_n x + \cos\text{h}\ \beta_n x - \frac{\cos\text{h}\ \beta_n L - \cos\ \beta_n L}{\sin\text{h}\ \beta_n L - \sin\ \beta_n L}(\sin\text{h}\ \beta_n x + \sin\ \beta_n x) \quad (2)$$

where β_n are values of β that solve Equation (3) [18]:

$$\cos \beta L \cos\text{h}\ \beta L = 1 \quad (3)$$

The equation of the torsional vibrations of the beam with a polar moment J and a modulus of rigidity G can be calculated as follows:

$$\rho J \frac{\partial^2 \phi(x,t)}{\partial t^2} - GK \frac{\partial^2 \phi(x,t)}{\partial x^2} = m_t(x,t) \quad (4)$$

$m_t(x,t)$ is the torque which is applied by the secondary suspensions on the car body. K is a torsional constant. The shape of the torsional modes of the free–free beam may be determined from Equation (5):

$$X_{n\phi}(x) = \cos \frac{n\pi}{L} x \quad (5)$$

2.2. Equation of Motion for Combined Rigid and Flexural Motion

The equations for the combined flexural–rigid motion of a vehicle body are formulated using three degrees of freedom (DOF). A schematic representation of the vehicle is shown in Figure 1. Presumably, the vehicle body and each bogie frame have three DOF of rigid body motion. These DOF are called pitch, vertical, and roll motions, respectively. In addition, flexible body motion is considered for the vehicle's body, as described in the preceding section. The wheelsets are considered rigid bodies, since they only have two DOF: the ability to move in a vertical and roll motion. The normal contact between the wheels and the rail is represented in this model as a linear spring.

Consider a railway vehicle consisting of a car body with mass m_c and moment of inertia J_{cx} and J_{cy} along the x and y axes, respectively. The car body is supported by two bogies, each with a frame of mass m_b, moment of inertia J_{bx} and J_{by} along the x and y axes, respectively, and a wheelset with mass m_w and moment of inertia J_{wx} along the x axis. L_b is the half distance between two bogies, L_w is the half distance among two wheelsets of the bogie, the car body has a length L, and L_c is centered at a longitudinal position. The front and rear secondary suspensions are located at longitudinal positions L_f and L_r, respectively. The lateral displacement of the secondary suspension is b, and b_w is the track gauge (half). The primary suspension axle has a vertical stiffness of k_p and a vertical damping of c_p. The secondary suspension for each side of the bogie has a vertical stiffness of k_s and a vertical damping of c_s. The equivalent linear spring of the Hertzian contact is k_{hz}. The railway vehicle has two flexible bending modes with damping constants ζ_{1z} and ζ_{2z} for the first and second modes, respectively, and a torsional mode with damping constant $\zeta_{1\phi}$.

Taking into account the model presented in Figure 1, the EOM that describes the behaviors of the vehicle body may be stated as follows:

$$m_c \ddot{z}_c = -f_{sfr} - f_{sfl} - f_{srr} - f_{srl} \quad (6)$$

$$I_{cy} \ddot{\theta}_c = L_b f_{sfr} + L_b f_{sfl} - L_b f_{srr} - L_b f_{srl} \quad (7)$$

$$I_{cx} \ddot{\phi}_c = -b f_{sfr} + b f_{sfl} - b f_{srr} + b f_{srl} \quad (8)$$

where f_{sij} is secondary suspension forces on the bogie frames and the vehicle body, respectively [18]. These forces may be defined using Equations (9)–(17).

$$\begin{aligned} f_{sfr} = k_s\Big[\Big(z_c + \sum\ X_{nz}\Big(L_f\Big)q_{nz} - L_b\theta_c + b\Big(\phi_c + \sum\ X_{n\phi}\Big(L_f\Big)q_{n\phi}\Big)\Big) - \Big(z_{bf} + b\phi_{bf}\Big)\Big] \\ + c_s\Big[\Big(\dot{z}_c + \sum\ X_{nz}\Big(L_f\Big)\dot{q}_{nz} - L_b\dot{\theta}_c + b\Big(\dot{\phi}_c + \sum\ X_{n\phi}\Big(L_f\Big)\dot{q}_{n\phi}\Big)\Big) - \Big(\dot{z}_{bf} + b\dot{\phi}_{bf}\Big)\Big] \end{aligned} \tag{9}$$

$$\begin{aligned} f_{sfr} = k_s\Big[\Big(z_c + \sum\ X_{nz}\Big(L_f\Big)q_{nz} - L_b\theta_c + b\Big(\phi_c + \sum\ X_{n\phi}\Big(L_f\Big)q_{n\phi}\Big)\Big) - \Big(z_{bf} + b\phi_{bf}\Big)\Big] \\ + c_s\Big[\Big(\dot{z}_c + \sum\ X_{nz}\Big(L_f\Big)\dot{q}_{nz} - L_b\dot{\theta}_c + b\Big(\dot{\phi}_c + \sum\ X_{n\phi}\Big(L_f\Big)\dot{q}_{n\phi}\Big)\Big) - \Big(\dot{z}_{bf} + b\dot{\phi}_{bf}\Big)\Big] \end{aligned} \tag{10}$$

$$\begin{aligned} f_{sfr} = k_s\Big[\Big(z_c + \sum\ X_{nz}\Big(L_f\Big)q_{nz} - L_b\theta_c + b\Big(\phi_c + \sum\ X_{n\phi}\Big(L_f\Big)q_{n\phi}\Big)\Big) - \Big(z_{bf} + b\phi_{bf}\Big)\Big] \\ + c_s\Big[\Big(\dot{z}_c + \sum\ X_{nz}\Big(L_f\Big)\dot{q}_{nz} - L_b\dot{\theta}_c + b\Big(\dot{\phi}_c + \sum\ X_{n\phi}\Big(L_f\Big)\dot{q}_{n\phi}\Big)\Big) - \Big(\dot{z}_{bf} + b\dot{\phi}_{bf}\Big)\Big] \end{aligned} \tag{11}$$

$$\begin{aligned} f_{sfr} = k_s\Big[\Big(z_c + \sum\ X_{nz}\Big(L_f\Big)q_{nz} - L_b\theta_c + b\Big(\phi_c + \sum\ X_{n\phi}\Big(L_f\Big)q_{n\phi}\Big)\Big) - \Big(z_{bf} + b\phi_{bf}\Big)\Big] \\ + c_s\Big[\Big(\dot{z}_c + \sum\ X_{nz}\Big(L_f\Big)\dot{q}_{nz} - L_b\dot{\theta}_c + b\Big(\dot{\phi}_c + \sum\ X_{n\phi}\Big(L_f\Big)\dot{q}_{n\phi}\Big)\Big) - \Big(\dot{z}_{bf} + b\dot{\phi}_{bf}\Big)\Big] \end{aligned} \tag{12}$$

where

$$\ddot{q}_{nz} + 2\zeta_{nz}\omega_{nz}\dot{q}_{nz} + \omega_{nz}^2 q_{nz} = \frac{2}{\rho AL}\Big[-f_{sfr}X_{nz}\Big(L_f\Big) - f_{sfl}X_{nz}\Big(L_f\Big) - f_{srr}X_{nz}(L_r) - f_{srl}X_{nz}(L_r)\Big] \tag{13}$$

$$\ddot{q}_{n\phi} + 2\zeta_{n\phi}\omega_{n\phi}\dot{q}_{n\phi} + \omega_{n\phi}^2 q_{n\phi} = \frac{2}{\rho JL}\Big[-bf_{sfr}X_{n\phi}\Big(L_f\Big) + bf_{sfl}X_{n\phi}\Big(L_f\Big) - bf_{srr}X_{n\phi}(L_r) + bf_{srl}X_{n\phi}(L_r)\Big] \tag{14}$$

The bogie frame EOM is given in Equations (15)–(17).

$$m_b\ddot{z}_{bi} = f_{sir} + f_{sil} - f_{pifr} - f_{pifl} - f_{pirr} - f_{pirl} \tag{15}$$

$$I_{by}\ddot{\theta}_{bi} = L_w f_{pifr} + L_w f_{pifl} - L_w f_{pirr} - L_w f_{pirl} \tag{16}$$

$$I_{bx}\ddot{\phi}_{bi} = bf_{sir} - bf_{sil} - bf_{pifr} + bf_{pifl} - bf_{pirr} + bf_{pirl} \tag{17}$$

The primary suspension forces between the bogie frames and axle boxes are denoted by f_{pjkl}, where j is an index that is to be replaced by either f or r to obtain the front or rear bogie primary suspension forces, respectively. These forces are defined in Equations (18)–(21).

$$f_{pifr} = k_p\Big[(z_{bi} - L_w\theta_{bi} + b\phi_{bi}) - \Big(z_{wif} + b\phi_{wif}\Big)\Big] + c_p[(\dot{z}_{bi} - L_w\dot{\theta}_{bi} + b\dot{\phi}_{bi}) - (\dot{z}_{wif} + b\dot{\phi}_{wif})] \tag{18}$$

$$f_{pifl} = k_p\Big[(z_{bi} - L_w\theta_{bi} - b\phi_{bi}) - \Big(z_{wif} - b\phi_{wif}\Big)\Big] + c_p[(\dot{z}_{bi} - L_w\dot{\theta}_{bi} - b\dot{\phi}_{bi}) - (\dot{z}_{wif} - b\dot{\phi}_{wif})] \tag{19}$$

$$f_{pirr} = k_p[(z_{bi} + L_w\theta_{bi} + b\phi_{bi}) - (z_{wir} + b\phi_{wir})] + c_p[(\dot{z}_{bi} + L_w\dot{\theta}_{bi} + b\dot{\phi}_{bi}) - (\dot{z}_{wir} + b\dot{\phi}_{wir})] \tag{20}$$

$$f_{pirl} = k_p[(z_{bi} + L_w\theta_{bi} - b\phi_{bi}) - (z_{wir} - b\phi_{wir})] + c_p[(\dot{z}_{bi} + L_w\dot{\theta}_{bi} - b\dot{\phi}_{bi}) - (\dot{z}_{wir} - b\dot{\phi}_{wir})] \tag{21}$$

The wheelset's EOM is given in Equation (22):

$$\begin{aligned} m_w\ddot{z}_{wij} &= f_{pijr} + f_{pijl} - (N_r + N_l)_{wij} \\ I_{wx}\ddot{\phi}_{wij} &= bf_{pijr} - bf_{pijl} - b_w(N_r - N_l)_{wij} \end{aligned} \tag{22}$$

The indexes i and j should be replaced by f and r to obtain equations for each front or rear wheelset or bogie, respectively. For instance, $\ddot{z}_{wfr}$ corresponds to the vertical acceleration of the rear wheelset of the front bogie. Additionally, N_r, and N_l represent the normal contact forces between the right and left wheels and the rail, respectively. These normal contact forces are different in Equation (23).

$$\begin{aligned} N_r &= k_{hz}\delta_r, \quad \delta_r = z_w + b_w\phi_w - z_{0r} \\ N_l &= k_{hz}\delta_l, \quad \delta_l = z_w - b_w\phi_w - z_{0l} \end{aligned} \tag{23}$$

2.3. Frequency Domain Analysis

The linear system of equations that was discussed in the prior section may be rewritten in the form of a matrix as $\ddot{X} + \mathbf{C}\dot{X} + \mathbf{K}X = \mathbf{D}Z_0$. In addition, $\mathbf{D}$ represents the stiffness matrix that is connected to the track excitation. Thus, the frequency response function matrix may be obtained using Equations (24)–(25).

$$\begin{aligned} \mathbf{H}(\omega) = & \left(-\mathbf{M}\omega^2 + j\omega\mathbf{C} + \mathbf{K}\right)^{-1} \\ & \mathbf{H}_d(\omega) = \mathbf{H}(\omega)\mathbf{D} \end{aligned} \tag{24}$$

Hence, the power spectral density (PSD) of the system's displacements may be calculated using Equation (25).

$$S_{Oi}(\omega) = \sum_{r=1}^{8}\sum_{s=1}^{8} \mathbf{H}^*_{dir}(\omega)\mathbf{S}_{Irs}(\omega)\mathbf{H}^{\mathrm{T}}_{dis}(\omega) \tag{25}$$

where $S_I(\omega)$ is the PSD matrix of the input excitation [19]. Equations (26)–(27) define the torsional irregularity (cross-level) and vertical irregularity of the track's center, respectively.

$$\tfrac{Z_r+Z_l}{2} = Z_v \tag{26}$$

$$\frac{Z_r - Z_l}{2} = Z_c \tag{27}$$

The cross-correlation and autocorrelation of the aforementioned inputs may be derived under the following assumptions [3,14,18,20,21]:

- Every kind of irregularity may be understood as a stationary random process that has no average.
- Gaussian distribution best describes the irregularity probability density.
- A range of wavelengths from 3 to 30 µm is used to determine spectral density.
- There is no link at all among the many anomalies that have been found.

By using autocorrelation, the system is able to calculate the autocorrelation and power spectral density (PSD) of the abnormalities perceived by each wheel, as shown in Equation (28):

$$\begin{gathered} R_i(\tau) = E[Z_i(t)Z_i(t+\tau)] = E[Z_v(t) + Z_c(t)Z_v(t+\tau) + Z_c(t+\tau)] = \\ E[Z_v(t)Z_v(t+\tau)] + E[Z_v(t)Z_c(t+\tau)] + E[Z_c(t)Z_v(t+\tau)] + E[Z_c(t)Z_c(t+\tau)] \end{gathered} \tag{28}$$

As a result, Equation (29) will be used to define the autocorrelation of the abnormalities associated with each wheel.

$$R_i(\tau) = R_v(\tau) + R_c(\tau) \tag{29}$$

where $R_v(\tau)$ and $R_c(\tau)$ are the vertical and roll autocorrelations of track abnormalities, respectively. In a similar manner, the PSD of the irregularities associated with each wheel may be computed, as described by Equation (30):

$$S_i(\omega) = S_v(\omega) + S_c(\omega) \tag{30}$$

where $S_v(\omega)$ and $S_c(\omega)$ represent the spectral density function (SDF) of the track's roll and the vertical components of abnormalities, respectively. Moreover, cross-SDF and cross-correlation between the right and left wheels of the wheelset can be calculated as

$$\begin{aligned} R_{RLi}(\tau) &= R_v(\tau) - R_c(\tau) \\ S_{RLi}(\omega) &= S_v(\omega) - S_c(\omega) \end{aligned} \tag{31}$$

The input cross-SDF of the irregularity can be calculated by Equation (32):

$$S_{ij}(\omega) = S_i(\omega)e^{-j\omega(x_j - x_i)/v} \tag{32}$$

The input cross-SDF is illustrated in Equation (33), when wheels are on different rails:

$$S_{RiLj}(\omega) = S_{RLi}(\omega)e^{-j\omega(x_j - x_i)/v} \tag{33}$$

Equation (34) is used to calculate the track irregularity for the roll and vertical components, as per RDDO guidelines:

$$\begin{aligned} S_v(\Omega) &= \frac{A_v\Omega_2^2(\Omega^2 + \Omega_1^2)}{\Omega^4(\Omega^2 + \Omega_2^2)} \\ S_c(\Omega) &= \frac{A_c\Omega_2^2}{(\Omega^2 + \Omega_1^2)(\Omega^2 + \Omega_2^2)} \end{aligned} \tag{34}$$

3. Rail Vehicle Performance Evaluation Index

The technique of selecting the fundamental DOF in the vehicle model, decreasing the DOF of the remaining nodes, and then extending the reduction result to the whole DOF is the foundation of the finite element substructure analysis. This approach may decrease the number of DOF as well as the size of the corresponding matrix, which all contribute to an increase in computing efficiency and an assurance of the associated calculation correctness [18]. There are several apparent benefits to using it for complicated dynamic computation.

The following is the dynamic equation that should be used for the vehicle structure:

$$[M]\{\ddot{q}\} + [C]\{\dot{q}\} + [K]\{q\} = Q \tag{35}$$

where $\{q\}, \{\dot{q}\}, \{\ddot{q}\}$ are the generalized coordinate column vectors representing the system's displacement, velocity and acceleration, respectively. The mass matrix of the flexible body is denoted by $[M]$. The matrices of stiffness are denoted by $[K]$. $[C]$ is the damping matrix. Q is the load vector, which includes the force of the force element, gravity, and any other external or internal loads.

After the selection of the master DOF, $\{q\}$ will be broken down into its component parts: the master DOF, denoted by $\{q_m\}$, and the dependent DOF, denoted by $\{q_s\}$. The dependent DOF may be modelled after the master DOF [22].

$$\{q_s\} = T\{q_m\} \tag{36}$$

where T is the transformation matrix that characterizes the connection between the master and dependent DOF.

Assuming that $\{q_m\}$ and $\{q_s\}$ are the order vectors m and s, and the transformation matrix is composed of m × s order vectors, q may be written as

$$q = \begin{bmatrix} q_m \\ q_s \end{bmatrix} = \begin{bmatrix} 0 \\ T \end{bmatrix} q_m = T * q_m \tag{37}$$

Hence, the equation for dynamic equilibrium may be written as follows:

$$\begin{bmatrix} M_{mm} M_{ms} \\ M_{sm} M_{ss} \end{bmatrix} \begin{Bmatrix} \grave{q}_m \\ \grave{q}_s \end{Bmatrix} + \begin{bmatrix} C_{mm} C_{ms} \\ C_{sm} C_{ss} \end{bmatrix} \begin{Bmatrix} \grave{q}_m \\ \grave{q}_s \end{Bmatrix} + \begin{bmatrix} K_{mm} K_{ms} \\ K_{sm} K_{ss} \end{bmatrix} \begin{Bmatrix} q_m \\ q_s \end{Bmatrix} = \begin{Bmatrix} Q_m \\ 0 \end{Bmatrix} \tag{38}$$

3.1. Running Stability

Running stability is a crucial factor for rail vehicles that determines their ability to maintain a stable and predictable motion. It is crucial for high-speed trains, wherein slight deviations from the intended path can have significant consequences. Running stability is affected by several factors, including the track parameters, the track surface condition, the train's speed, and the train's characteristics, such as its weight distribution and suspension system. To ensure running stability, rail vehicles are designed to have low centres of gravity and effective suspension systems, which help to reduce the impact of external forces and maintain the stability of the train. Additionally, track geometry and surface conditions are carefully monitored and maintained to minimize the risk of sudden changes in direction or unwanted oscillations. Advanced monitoring systems and automated control technologies are also employed to detect and correct deviations from the intended path, helping to ensure that rail vehicles remain stable and safe at all times. Running stability is critical to the safe and efficient operation of rail vehicles, and rail operators make significant efforts to maintain it at all times. This evaluation is carried out by the running stability. The stability index is shorthand for the Sperling index, broken down into vertical and horizontal stability. The Sperling Ride Index is a widely used measure of ride comfort in railway engineering. The index is based on the vertical acceleration experienced by a passenger on a train, and considers the frequency range of the vibrations [23].

The Sperling Ride Index [24] is calculated by first measuring the vertical acceleration experienced by a passenger on a train using an accelerometer. The acceleration is then filtered to remove high-frequency noise and vibrations. The filtered acceleration data are then integrated twice to obtain the displacement of the passenger in the vertical direction. This displacement is then compared to a standardized curve representing passengers' minimum discomfort threshold. The level of ride comfort may be determined with the help of Equation (39) [3].

$$W_z = 0.896 \sqrt[10]{\frac{a^3}{f} F(f)} \tag{39}$$

where a is the acceleration of the vibration, and frequency is denoted by the letter f. The weighting coefficient associated with vibration frequency is denoted by the symbol $F(f)$. Since the vibration caused by the real vehicle moving down the track is unpredictable, the data must be categorized on the acceleration caused by the vibration in accordance with the frequency, and the total overall stability index W_{tot} must be determined. The comfort index is given in Figure 2.

$$W_{tot} = \left(W_1^{10} + W_2^{10} + W_3^{10} + \cdots + W_n^{10}\right)^{0.1} \tag{40}$$

3.2. Running Safety

Running safety is a critical aspect of rail vehicle operations. It involves ensuring the vehicle operates safely and reliably on the track while minimizing the risk of accidents or incidents. When referring to a vehicle's performance, "running safety" refers to the performance that ensures the vehicle will not cause overturning, derailment or damage to the track when operating within the range of speeds that correspond to its maximum running speed [3]. The wheel load reduction rate, derailment coefficient, and other metrics are among the most critical components of the running safety index RDSO mandates on the Indian Railway.

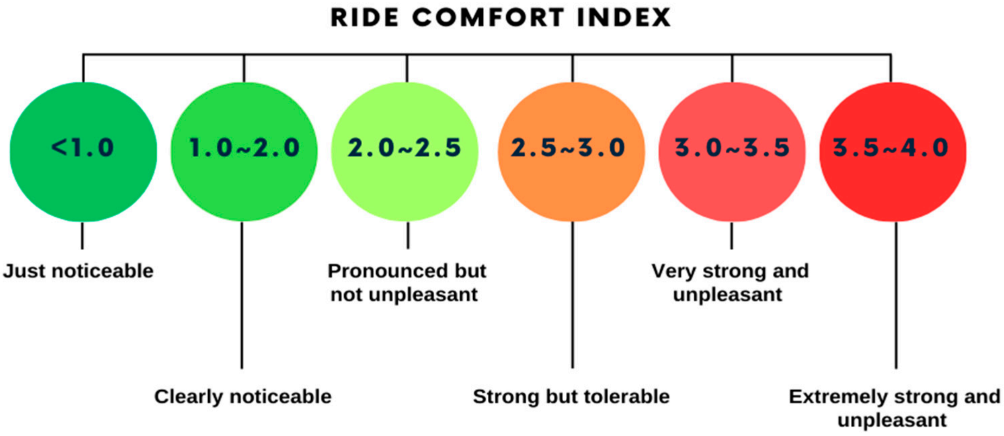

Figure 2. Sperling Ride Index.

3.2.1. Derailment Analysis

The act of a railway car running off its tracks is meant to be understood as a derailment; it can be caused by collision with another item, the mechanical failure of tracks (such as broken rails and track geometry misalignment), the mechanical failure of wheels, and environmental pressures [25]. A derailment occurs when a train's wheels leave the track, resulting in a loss of control and potential damage to the train, its cargo, and the surrounding area. There are various factors affecting it, including track defects, mechanical failures, excessive speed, operator errors, and external forces such as weather events or collisions. The consequences of a derailment can range from minor disruptions to significant injuries, fatalities, and environmental damage, depending on the severity of the incident. As a result, rail operators and regulators prioritize preventing derailments through rigorous maintenance and inspection protocols and improved technology. While analyzing the operational safety of the vehicle model, the derailment quotient is one of the metrics considered [3].

As a railway car navigates a curve, the contact forces exerted by the leading wheelset in the system are much greater than those exercised by the remaining wheelsets. Hence, to study running safety, the "derailment quotient" of the left wheel of the leading wheelset is applied, as stated in Equation (41):

$$\frac{Q}{P} = \frac{\tan \partial - \mu}{1 + \mu \tan \partial} \tag{41}$$

where P = vertical force, and Q = transverse force of rail-wheel.

3.2.2. Wheel Load Reduction Rate

The wheel load reduction rate is an essential factor for rail vehicles that directly impacts their performance and safety. The reduction rate refers to the amount of force that is removed from the wheels of a train as it passes over an uneven track or encounters other types of irregularities [26–28]. This is particularly important because the train's weight can cause excessive wear and tear on the track, leading to damage that can increase the likelihood of derailment or other accidents. To reduce the wheel load, rail vehicles are often equipped with various technologies such as air suspension systems, which allow the train to adjust its height and distribute its weight more evenly [29,30]. Additionally, track maintenance programs are implemented to ensure that tracks are regularly inspected and repaired to prevent further damage. By reducing the wheel load and implementing effective maintenance strategies, rail operators can improve the performance and safety of their trains, increase their longevity, and minimize the risk of accidents on the tracks. The wheel load-reduction rate is another derailment safety factor and can be calculated using Equation (42):

$$\frac{\Delta p}{\overset{\leftharpoonup}{p}} = \frac{|P_R - P_L|/2}{p_{st}} \tag{42}$$

4. Experimental Analysis

An on-track vibration test was created to obtain better knowledge of the vibration transition between primary and secondary suspension systems, as well as the coupled shaking between the suspended equipment and its vehicle body. Accelerometers and displacement sensors were used to monitor accelerations on the bogie frame, wheelset axle-box, and connections between the vehicle body and the suspended equipment and its vehicle body [6]. These sensors were linked by cables to the data collection system in the equipment cabin. The on-track vibration test was developed to capture the vehicle dynamics over a protracted period continuously [31–33]. The vibration characteristics of the equipment are examined and illustrated in Figure 3.

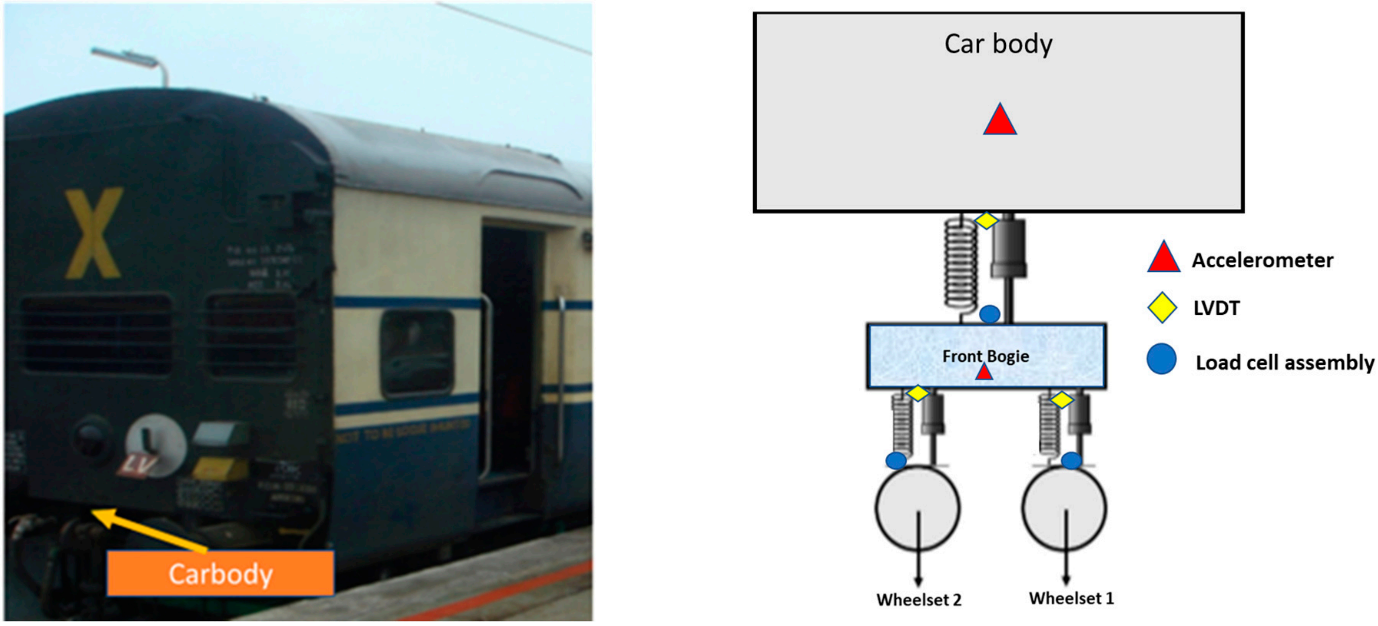

(**a**) (**b**)

Figure 3. (**a**) Rail vehicle test coach for experimental evaluation; (**b**) location of the different sensors for collecting data.

After measuring the accelerations of the equipment and the vehicle body in response to various bogie running performances, the vibration source and spectrum composition were analyzed. On a designated stretch of the IR track between Palwal and Mathura, the rolling stock is put through its paces at maximum speeds ten per cent faster than regular operating rates. Oscillation tests were carried out on a track in good condition at different speeds [34,35].

The frame acceleration passband frequency range is 0.5 to 12 Hz, while the frame acceleration sampling frequency is 2 kHz. The acceleration measurement device has a passband frequency range of 0.1–200 Hz and a sampling frequency of 1 kHz. An oscillation test performed on the real-world environment by RDSO validates the numerical model. The proposed numerical passive model's ride comfort for passengers is particularly compared to the experimental data acquired by RDSO [6]. RDSO was the organization that conducted the experiments. Oscillation trials are a form of on-track testing performed using a prototype coach that is equipped to record displacement, acceleration, events, and speed. Throughout the oscillation tests, the maximum vertical and lateral ride indices in both unladen and laden states were determined. The RDSO Sperling Ride Index method was used to compute the riding index. The value of the riding index, according to the RDSO Sperling Ride Index, was lower than 2.75 but still between 3.25 and 3.50 at most, with 3.25 being the preferred range. It was determined that the riding behavior of the same was adequate [36]. Yet, there is room for improvement in the ride index values. The experimental ride index and the numerical ride index are compared in Figure 4, which illustrates the comparison results under unladen and laden settings, respectively. Additionally, the findings generated from the numerical analysis of the suggested model have attained an excellent general agreement with the experimentally measured results. This can be seen by comparing the two sets of data. The difference in the riding index may be attributed, in large part, to factors that were omitted from consideration to simplify the mathematical model.

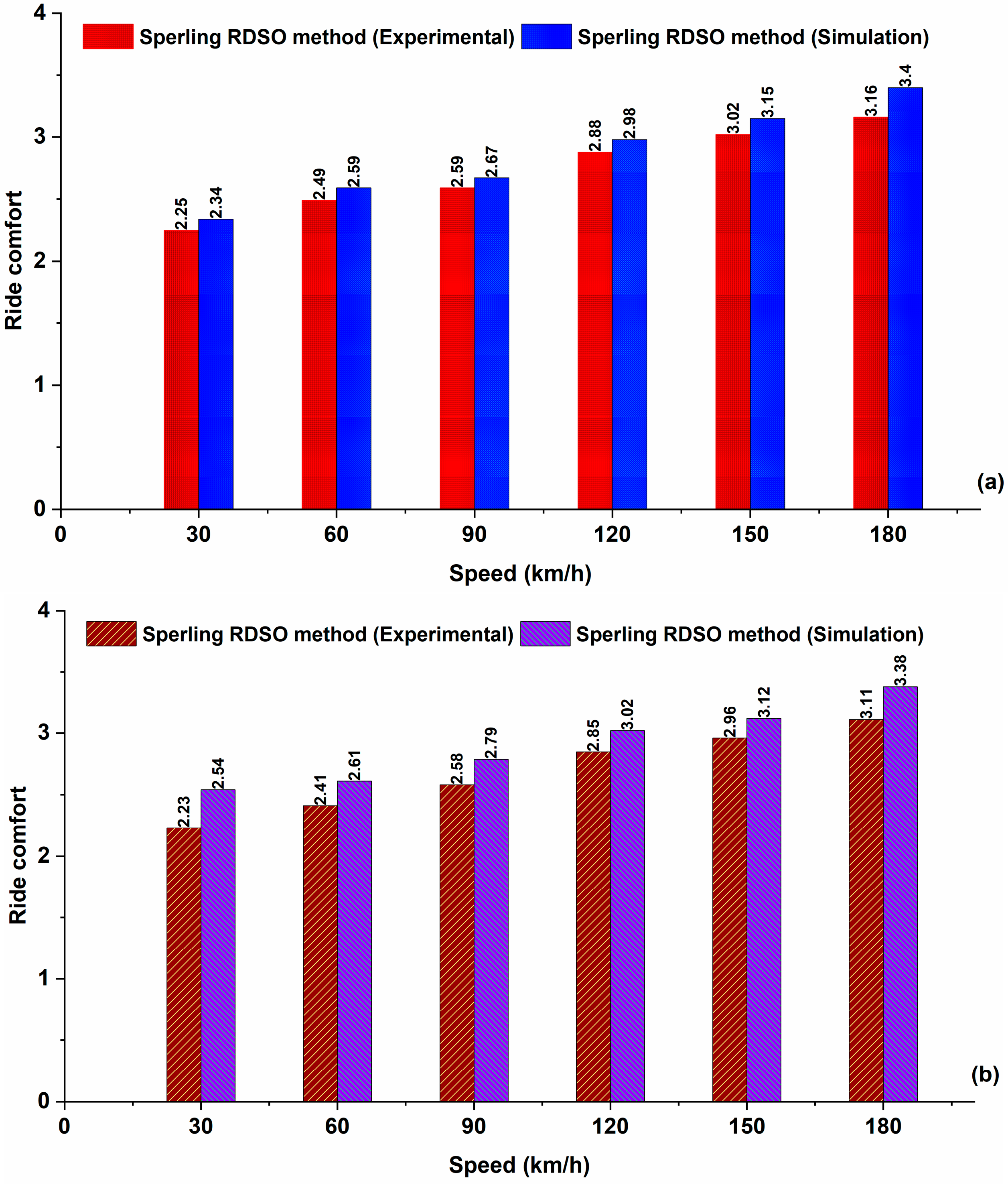

Figure 4. Numerical–experimental comparison for (**a**) the unladen and (**b**) the laden state.

5. Results and Discussion

The rigid body dynamics model treats the numerous components of the vehicle system as if they were a single rigid body. This model disregards the local vibration in each element, instead focusing on how the components are connected. The rigid and flexible coupling dynamic model produces a one-of-a-kind dynamic effect. This effect can take into account the coupling between the object's rigid body motion and the component's elastic deformation, in addition to the one-of-a-kind dynamic effect brought about by the coupling. The traditional rigid and flexible coupling model will only consider one member of the vehicle system to be an elastic body, while the other component will remain rigid. This will allow for a more precise study of the wheel abrasion caused by the dynamic performance of the vehicle body, frame, and wheel parts, all considered elastic bodies. This will allow for the combination of a vehicle model with flexible construction. The research establishes a stiff flexible coupled dynamic model of an ICF railway coach vehicle by combining finite element analysis with multi-body dynamics simulation. This model is depicted in Figure 5.

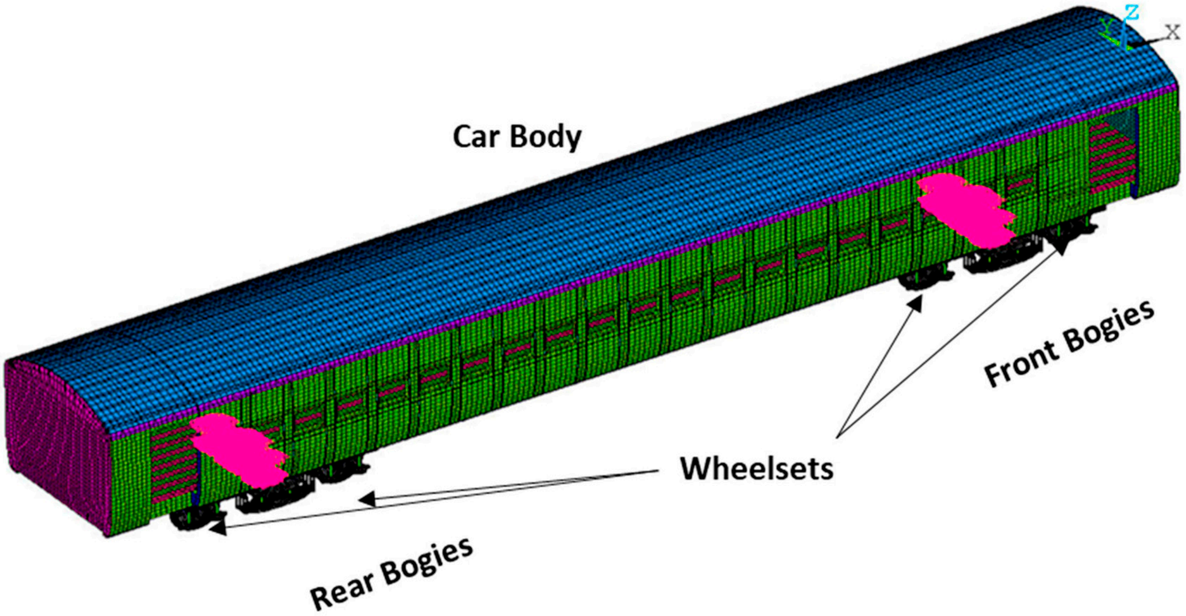

Figure 5. 3D FEA model of rail vehicle.

The comprehensive rigid–flexible coupling model of the ICF railway coach is created using a geometric model formulated in UNIGRAPHICS NX7.5, which is exported in Parasolid format to HYPERMESH 10 to develop the finite element model of the coach. The Parasolid format is preferred for its effective translation of solid models into ANSYS-17 FEA software. HYPERMESH is chosen due to its faster computing ability and interoperability with ANSYS in terms of element types and file extensions. The meshed coach model in HYPERMESH 10 is further exported to ANSYS Mechanical APDL in cdb (card scan database) format to conduct the finite element analysis.

The idealized railway coach model is obtained by considering the car body shell with various channel sections, two bogie assemblies on either end, a trough floor with cross beams, and body bolsters on front and rear ends, while neglecting remaining parts. The solid components of the coach, bogie frame, body bolsters, wheel axle sets and bogie bolster are discretized using the SOLID 45 element type in HYPERMESH 10. The coach shell with the channels, such as stanchions and sole-bars, is meshed using SHELL 63 in HYPERMESH 10. The suspensions between the car body of the coach and the bolsters are defined using the line element type COMBIN14, accounting for both the helical spring and the damping. For compatibility, the shell and solid elements are integrated using the option 'Coupling' in

ANSYS Preprocessor. After achieving mesh convergence, the finite element model of the railway coach comprises 171,677 elements and 204,027 nodes.

5.1. Substructure Analysis

The flexible modes or eigenmodes of the car body were investigated in this study. The results showed that the first vertical bending mode had a frequency of 12.14 Hz. This mode corresponds to the vertical deflection of the car body along the longitudinal axis. The first lateral bending mode had a frequency of 14.25 Hz, corresponding to the car body's lateral deflection along the transverse axis. Finally, the first torsion mode had a frequency of 19.87 Hz, corresponding to the car body's twisting deformation along the vertical axis. These flexible modes are important to consider when analyzing the dynamic behavior of the car body, as they can affect the ride quality and safety of the passengers. This analysis provides valuable information for the design and optimization of railway vehicles, especially in terms of reducing vibrations and improving passenger comfort. Table 1 shows the different first-mode shapes with frequency.

Table 1. Mode shape of railway vehicle car body.

S. R. No	Modes	Frequencies (Hz)
1	First vertical bending	12.14
2	First lateral bending	14.25
3	First torsion	19.87

5.2. Acceleration Response

The acceleration response at the vehicle body's mass center for both the rigid and flexible car body centers was compared at speeds ranging from 60 km/h to 180 km/h. The results show that for all speeds, the acceleration response was higher for the flexible car body than for the rigid car body. At 60 km/h, the acceleration response for the flexible car body was 0.54 m/s^2, while for the rigid car body, it was 0.48 m/s^2. Similarly, at 120 km/h, the acceleration response for the flexible car body was 0.68 m/s^2, while for the rigid car body, it was 0.59 m/s^2. At higher speeds of 150 km/h and 180 km/h, the difference in acceleration response between the two car bodies was even more significant, as shown in Figure 6. The dissimilarities between the real high-speed train vehicle and the rigid model arise from the fact that the train's car body experiences flexible resonances stimulated by track irregularities or bogie system vibration, which cannot be accurately accounted for in a rigid model.

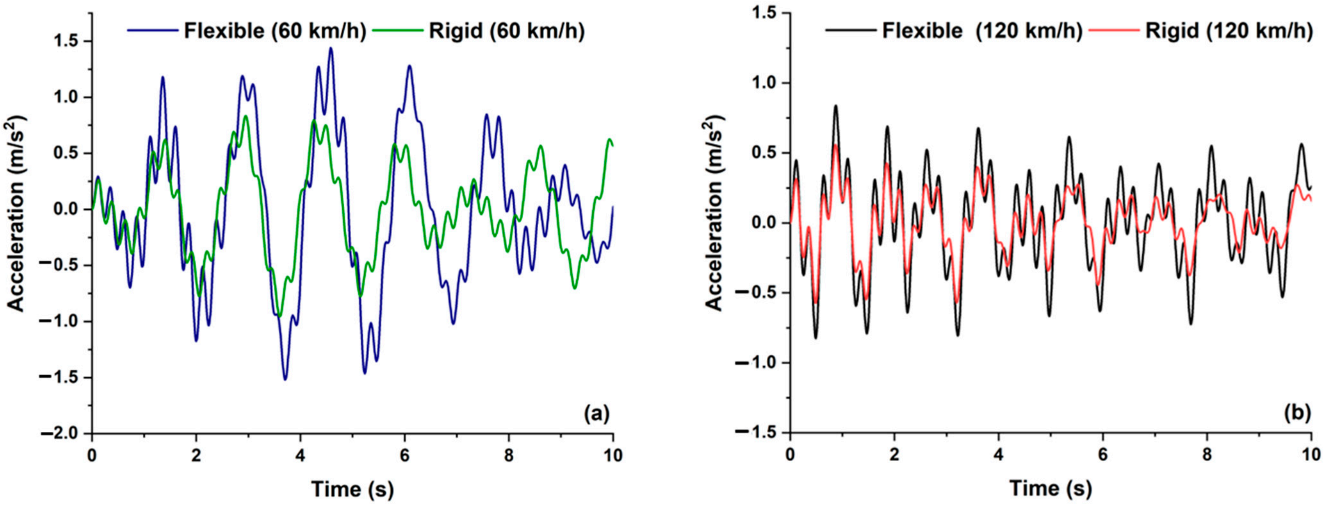

Figure 6. *Cont.*

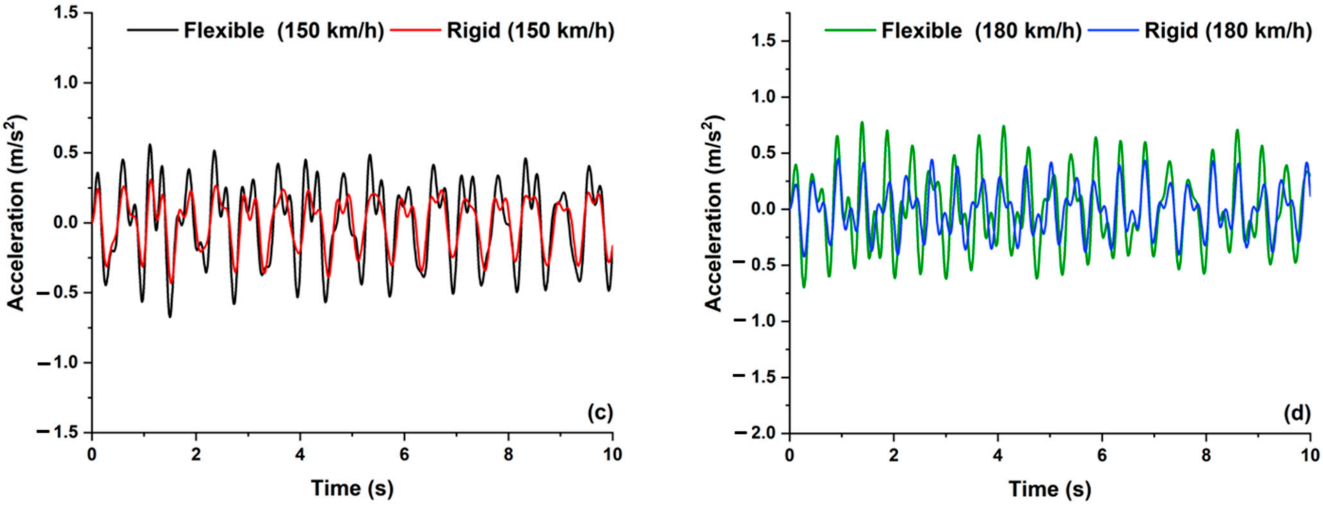

Figure 6. Acceleration response near the vehicle body's mass center (**a**) 60 km/h. (**b**)120 km/h. (**c**) 150 km/h. (**d**) 180 km/h.

5.3. Running Comfort

To examine vehicle response considering car body flexibility and to compare it with a rigid car body model, vehicle simulation speeds are considered from 30 km/h to 180 km/h. For the simulation of the running comfort, the Sperling Ride Index method is used for the vehicle system, and the track spectrum of the dedicated Mathura to Palwal line is used. The variations in ride quality at the car body center and end for bending frequency for different car body damping ratio values are shown in Figures 7 and 8, respectively. Figure 7 indicates that for car body bending frequencies below 7.5 Hz, the car body vibrations are very high, and the resonance is observed at a frequency of nearly 6.4 Hz. With car body damping factors ζ = 0, 0.02, 0.03 and 0.05, the ride index at resonating frequency at the center is observed to be 2.84, 2.52, 2.42, 2.2, respectively, which indicates that the damping factor has isolation effects on the resonance peak. With car body damping factors ζ = 0, 0.02, 0.03 and 0.05, the ride index at resonating frequency at the end is observed to be 3.27, 3.03, 2.87, and 2.65, respectively (Figure 8). Figures 7 and 8 also suggest that when the damping factor is increased from 2% to 5%, the ride index is reduced to nearly 12.7%. Field test reports have indicated that the car body damping factor of a loaded car body in India is nearly 2.5%, and a further increase in this value requires an advanced car body design.

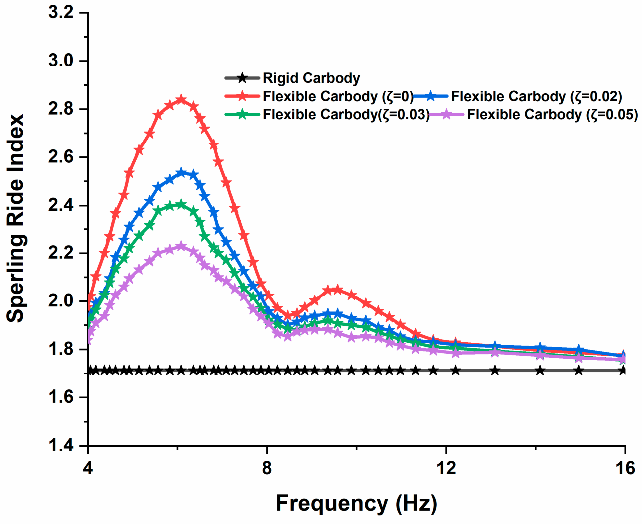

Figure 7. The Sperling Ride Index at the rigid and flexible car body center.

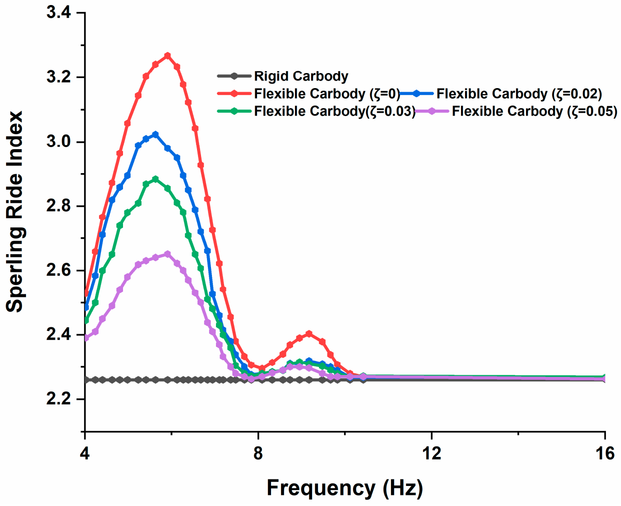

Figure 8. The Sperling Ride Index at the rigid and flexible car body end.

The car body damping factor is limited to 2.5%. Therefore, the other substitute for the isolating car body flexural vibrations raises its first bending frequency. Figures 6 and 7 also indicate that when the frequency in the first bending mode is more than 10 Hz, the ride index for the end of the flexible and the rigid car body is identical. At the center, the ride index value of the flexible car body approaches that of the rigid car body, irrespective of the value of the damping factor. At 7 Hz and a damping factor of 2%, the ride index is nearly 2.4, which is acceptable.

The simulation results using the Sperling Ride Index are compared with the experimental results and shown in Table 2. It can be seen from the table that the ride comfort for the considered speed varies from 2.54 to 3.38 for the RF simulation and 2.2 to 3.3 for the MR simulation. Field test reports have indicated that the ride comfort varies from 2.2 to 3. Hence, when comparing the experimental results, the % error for RF varies from 4 to 14 %, and for MR, it varies from 0.4 to 6%.

Table 2. Calculation error of Sperling Ride Index.

Speed (Km/h)	Rigid–Flexible Simulation (RF)	Multi-Rigid Simulation (MR)	Experimental (E)	% Error = $\left(\frac{E-RF}{E}\right) * 100$	% Error = $\left(\frac{E-MR}{E}\right) * 100$
30	2.54	2.24	2.2	13.90	0.45
60	2.61	2.47	2.4	8.30	2.49
90	2.79	2.67	2.5	8.14	3.49
120	3.02	2.94	2.8	5.96	3.16
150	3.12	3.04	2.9	5.41	2.70
180	3.38	3.28	3	8.68	5.47

5.4. Running Safety

To perform the running stability simulation, the tried-and-true rigid–flexible coupled vehicle model and the multi-body model are used. As a result, derailments and a wheel load reduction rate were examined so that the running safety could be assessed. It is known that extreme vehicle hunting may result in the vehicle body colliding laterally with the road. Moreover, it may result in the wheel flange colliding laterally with the rail.

In the second scenario, there is a risk that the vehicle may be derailed. For this reason, it is essential to research the impact of derailing utilizing models of rigid–flexible coupled vehicles and multi-body models. The Nadal restriction is applied for these specific objectives. The comparison of the data from the simulation with the outcomes of the experiment is shown in Table 3.

Table 3. Calculation error of running safety as a mean derailment coefficient.

Speed (Km/h)	Rigid–Flexible Simulation (RF)	Multi-Rigid Simulation (MR)	Experimental (E)	% Error = $\left(\frac{E-RF}{E}\right) * 100$	% Error = $\left(\frac{E-MR}{E}\right) * 100$
30	0.104	0.101	0.112	7.143	9.821
60	0.117	0.112	0.129	9.302	13.178
90	0.128	0.119	0.136	5.882	12.500
120	0.134	0.124	0.142	5.634	12.676
150	0.141	0.139	0.155	9.278	10.112
180	0.170	0.167	0.183	6.944	8.616

Table 3 shows that the derailment coefficient for the considered speed varies from 0.104 to 0.170 for the RF simulation and 0.104 to 0.167 for the MR simulation. Field test reports have indicated that the mean derailment coefficient varies from 0.112 to 0.183. Hence, when comparing the experimental results, the % error for RF varies from 5 to 9%, and for MR, it varies from 8 to 14%. Therefore, the mean derailment coefficient of the vehicle body in terms of error for the rigid body dynamics model is more than the modulus value obtained by the rigid–flexible coupling dynamic model. Similarly, for the mean wheel load reduction rate, Table 4 shows the comparison of simulation data with the experimental results.

Table 4. Calculation error of running safety as a mean wheel load reduction rate.

Speed (Km/h)	Rigid–Flexible Simulation (RF)	Multi-Rigid Simulation (MR)	Experimental (E)	% Error = $\left(\frac{E-RF}{E}\right) * 100$	% Error = $\left(\frac{E-MR}{E}\right) * 100$
30	0.124	0.121	0.129	3.876	6.202
60	0.139	0.130	0.146	4.795	10.959
90	0.145	0.139	0.154	5.844	9.740
120	0.157	0.147	0.169	7.101	13.018
150	0.179	0.180	0.209	14.552	13.895
180	0.221	0.219	0.247	10.366	11.541

Table 4 suggests that the mean wheel load reduction rate for the considered speed varies from 0.124 to 0.221 for the RF simulation and 0.121 to 0.219 for the MR simulation. Field test reports have indicated that the mean derailment coefficient varies from 0.129 to 0.247. Hence, when comparing the experimental results, the % error for RF varies from 3 to 15%, and for MR, it varies from 6 to 14%. Therefore, the mean derailment coefficient and mean wheel load reduction rate of the vehicle body in terms of error for the rigid body dynamics model is more than the modulus value obtained by the rigid–flexible coupling dynamic model.

6. Conclusions

Flexible–rigid rail vehicles are characterized by a combination of rigid and flexible components which interact with each other to determine the vehicle's behaviors. An important aspect of experimental and numerical analysis is accurately modelling these interactions and identifying ways to improve them. This can involve analyzing the behaviors of flexible components, such as the car body and bogie, and their interaction with rigid components, such as the wheels and track. The dynamic response of a rail vehicle using experimental and simulation analysis on a multi-rigid–flex body model was investigated. A mathematical model is developed by keeping the bogie frame and wheelsets rigid, and the car body is used as a flexible and rigid body, respectively. ANSYS is used to build a finite element model for the car body, and substructure and modal analyses are performed. The mathematical model is validated through the experiment conducted by RDSO. Based on the substructure analysis, it has been determined that the first vertical bending frequency of the system is 12.14 Hz, the first lateral bending frequency is 14.25 Hz, and the first torsion frequency is 19.87 Hz. Comparing the experimental and simulation results for the considered speed range of 30–180 km/h using the Sperling Ride Index has shown that the ride comfort, mean derailment coefficient, and mean wheel load reduction rate varies for both RF and MR simulations. The % error for the RF simulation in ride comfort varies from 4 to 14%, in mean derailment coefficient from 5 to 9%, and in mean wheel load reduction rate from 3 to 15%. The % error for the MR simulation in ride comfort varies from 0.4 to 6%, in mean derailment coefficient from 8 to 14%, and in mean wheel load reduction rate from 6 to 14%. Therefore, using a rigid–flexible coupling dynamic model provides more accurate results than the rigid body dynamics model in terms of mean derailment coefficient and mean wheel load reduction rate. The simulation result shows that the elastic vibration may not be ignored in the vehicle dynamics, because the rigid–flexible coupling model is marginally larger than the rigid-body model of ride comfort and safety compared with experimental results.

Author Contributions: S.K.S. and R.C.S. prepared the inspection system for the experiment and performed the experiments presented in this research. J.L. conceived the original idea. J.L. designed the methodology, gave guidance, and helped to improve the quality of the manuscript. S.K.S. wrote the original draft preparation in consultation with Y.C., who reviewed and edited the final manuscript. All authors have read and agreed to the published version of the manuscript.

Funding: This work was supported by a National Research Foundation of Korea (NRF) grant funded by the Korea government (MSIT) (No. 2019R1A5A8083201) and Korea Institute of Energy Technology Evaluation and Planning (KETEP) grant funded by the Korea government (MOTIE) (20214000000480, Development of R&D engineers for combined cycle power plant technologies), No. 2020R1G1A1011142).

Data Availability Statement: Not applicable.

Conflicts of Interest: The authors declare no conflict of interest.

References

1. Sharma, S.K.; Sharma, R.C.; Lee, J. Effect of Rail Vehicle–Track Coupled Dynamics on Fatigue Failure of Coil Spring in a Suspension System. *Appl. Sci.* **2021**, *11*, 2650. [CrossRef]
2. Bokaeian, V.; Rezvani, M.A.; Arcos, R. The coupled effects of bending and torsional flexural modes of a high-speed train car body on its vertical ride quality. *Proc. Inst. Mech. Eng. Part K J. Multi-Body Dyn.* **2019**, *233*, 979–993. [CrossRef]
3. Zhang, M.; Li, X.; Liu, X. Dynamic performance analysis of a urban rail vehicle based on rigid-flexible coupling. *AIP Conf. Proc.* **2019**, *2073*, 020012. [CrossRef]
4. Wu, Q.; Cole, C.; Spiryagin, M.; Chang, C.; Wei, W.; Ursulyak, L.; Shvets, A.; Murtaza, M.A.; Mirza, I.M.; Zhelieznov, K.; et al. Freight train air brake models. *Int. J. Rail Transp.* **2023**, *11*, 1–49. [CrossRef]
5. Sharma, R.C.; Sharma, S.; Sharma, S.K.; Sharma, N.; Singh, G. Analysis of bio-dynamic model of seated human subject and optimization of the passenger ride comfort for three-wheel vehicle using random search technique. *Proc. Inst. Mech. Eng. Part K J. Multi-Body Dyn.* **2021**, *235*, 106–121. [CrossRef]
6. Sharma, S.K.; Sharma, R.C.; Lee, J.; Jang, H.-L. Numerical and Experimental Analysis of DVA on the Flexible-Rigid Rail Vehicle Carbody Resonant Vibration. *Sensors* **2022**, *22*, 1922. [CrossRef]
7. Kozek, M.; Benatzky, C.; Schirrer, A.; Stribersky, A. Vibration damping of a flexible car body structure using piezo-stack actuators. *Control Eng. Pract.* **2011**, *19*, 298–310. [CrossRef]
8. Kamada, T.; Hiraizumi, K.; Nagai, M. Active vibration suppression of lightweight railway vehicle body by combined use of piezoelectric actuators and linear actuators. *Veh. Syst. Dyn.* **2010**, *48*, 73–87. [CrossRef]
9. Huang, C.; Zeng, J.; Luo, G.; Shi, H. Numerical and experimental studies on the car body flexible vibration reduction due to the effect of car body-mounted equipment. *Proc. Inst. Mech. Eng. Part F J. Rail Rapid Transit* **2018**, *232*, 103–120. [CrossRef]
10. Foo, E.; Goodall, R.M. Active suspension control of flexible-bodied railway vehicles using electro-hydraulic and electro-magnetic actuators. *Control Eng. Pract.* **2000**, *8*, 507–518. [CrossRef]
11. Wang, Q.; Zeng, J.; Wu, Y.; Zhu, B. Study on semi-active suspension applied on carbody underneath suspended system of high-speed railway vehicle. *J. Vib. Control* **2020**, *26*, 671–679. [CrossRef]
12. Beltran-Carbajal, F.; Valderrabano-Gonzalez, A.; Favela-Contreras, A.; Hernandez-Avila, J.L.; Lopez-Garcia, I.; Tapia-Olvera, R. An Active Vehicle Suspension Control Approach with Electromagnetic and Hydraulic Actuators. *Actuators* **2019**, *8*, 35. [CrossRef]

13. Bhardawaj, S.; Sharma, R.; Sharma, S. Ride Analysis of Track-Vehicle-Human Body Interaction Subjected to Random Excitation. *J. Chin. Soc. Mech. Eng.* **2020**, *41*, 236–237. [CrossRef]
14. Sun, W.; Zhou, J.; Gong, D.; You, T. Analysis of modal frequency optimization of railway vehicle car body. *Adv. Mech. Eng.* **2016**, *8*, 168781401664364. [CrossRef]
15. Sun, Y.; Zhou, J.; Gong, D.; Sun, W.; Xia, Z. A New Vibration Absorber Design for Under-Chassis Device of a High-Speed Train. *Shock Vib.* **2017**, *2017*. [CrossRef]
16. Dumitriu, M. Influence of Suspended Equipment on the Carbody Vertical Vibration Behaviour of High-Speed Railway Vehicles. *Arch. Mech. Eng.* **2016**, *63*, 145–162. [CrossRef]
17. Miao, B.R.; Luo, Y.X.; Peng, Q.M.; Qiu, Y.Z.; Chen, H.; Yang, Z.K. Multidisciplinary design optimization of lightweight carbody for fatigue assessment. *Mater. Des.* **2020**, *194*, 108910. [CrossRef]
18. Deng, Y.; Zhao, Y.; Xu, H.; Lin, F.; Wang, Q. Rigid-flexible coupling modelling and dynamic performance analysis of novel flexible road wheel. *Proc. Inst. Mech. Eng. Part K J. Multi-Body Dyn.* **2020**, *234*, 67–81. [CrossRef]
19. Han, J.; Zhong, S.Q.; Zhou, X.; Xiao, X.B.; Zhao, G.T.; Jin, X.S. Time-domain model for wheel-rail noise analysis at high operation speed. *J. Zhejiang Univ. Sci. A* **2017**, *18*, 593–602. [CrossRef]
20. Gong, D.; Sun, W.; Zhou, J.; Xie, X. Analysis on the vertical coupled vibration between bogies and metro car body. *Procedia Eng.* **2011**, *16*, 825–831. [CrossRef]
21. Wang, Y. Analysis of Vehicle Sperling Index Compared with the Flexible-rigid Coupled Model and Multi-body Rigid Model. In Proceedings of the 7th International Conference on Management, Education, Information and Control (MEICI 2017), Shenyang, China, 15–17 September 2017; Volume 156, pp. 237–244. [CrossRef]
22. Yang, S.; Li, F.; Shi, H.; Wu, P.; Zeng, J. A roll frequency design method for underframe equipment of a high-speed railway vehicle for elastic vibration reduction. *Veh. Syst. Dyn.* **2022**, *60*, 2211–2230. [CrossRef]
23. Carlbom, P. *Carbody and Passengers in Rail Vehicle Dynamics*; Royal Institute of Technology: Stockholm, Sweden, 2000.
24. Jeniš, F.; Kubík, M.; Michálek, T.; Strecker, Z.; Žáček, J.; Mazůrek, I. Effect of the Magnetorheological Damper Dynamic Behaviour on the Rail Vehicle Comfort: Hardware-in-the-Loop Simulation. *Actuators* **2023**, *12*, 47. [CrossRef]
25. Indian Railways Institute of Civil Engineering the Investigation of Derailments. 2007; pp. 1–353. Available online: https://iricen.gov.in/iricen/books_jquery/investigations_of_derailments_2015 (accessed on 23 January 2023).
26. Sharma, R.C.; Palli, S.; Sharma, N.; Sharma, S.K. Ride Behaviour of a Four-wheel Vehicle using H Infinity Semi-active Suspension Control under Deterministic and Random Inputs. *Int. J. Veh. Struct. Syst.* **2021**, *13*, 234–237. [CrossRef]
27. Bhardawaj, S.; Sharma, R.C.; Sharma, S.K. Analysis of frontal car crash characteristics using ANSYS. *Mater. Today Proc.* **2020**, *25*, 898–902. [CrossRef]
28. Sharma, S.K.; Sharma, R.C.; Sharma, N. Combined Multi-Body-System and Finite Element Analysis of a Rail Locomotive Crashworthiness. *Int. J. Veh. Struct. Syst.* **2020**, *12*. [CrossRef]
29. Bhardawaj, S.; Chandmal Sharma, R.; Kumar Sharma, S. A Survey of Railway Track Modelling. *Int. J. Veh. Struct. Syst.* **2019**, *11*, 508–518. [CrossRef]
30. Sharma, S.K.; Sharma, R.C. Pothole Detection and Warning System for Indian Roads. In *Advances in Interdisciplinary Engineering*; Springer: Singapore, 2019; pp. 511–519.
31. Sharma, S.K.; Kumar, A. The Impact of a Rigid-Flexible System on the Ride Quality of Passenger Bogies Using a Flexible Carbody. In Proceedings of the Proceedings of the Third International Conference on Railway Technology: Research, Development and Maintenance, Stirlingshire, UK, 5–8 April 2016; Pombo, J., Ed.; Civil-Comp Press: Stirlingshire, UK, 2016; p. 87.
32. Sharma, S.K.; Lee, J.; Jang, H.-L. Mathematical Modeling and Simulation of Suspended Equipment Impact on Car Body Modes. *Machines* **2022**, *10*, 192. [CrossRef]
33. Sharma, S.K.; Lee, J. Crashworthiness Analysis for Structural Stability and Dynamics. *Int. J. Struct. Stab. Dyn.* **2021**, *21*, 2150039. [CrossRef]
34. Sharma, S.K.; Lee, J. Design and Development of Smart Semi Active Suspension for Nonlinear Rail Vehicle Vibration Reduction. *Int. J. Struct. Stab. Dyn.* **2020**, *20*, 2050120. [CrossRef]
35. Sharma, S.K.; Phan, H.; Lee, J. An Application Study on Road Surface Monitoring Using DTW Based Image Processing and Ultrasonic Sensors. *Appl. Sci.* **2020**, *10*, 4490. [CrossRef]
36. Sharma, S.K.; Kumar, A. Impact of Longitudinal Train Dynamics on Train Operations: A Simulation-Based Study. *J. Vib. Eng. Technol.* **2018**, *6*, 197–203. [CrossRef]